Nonstationary statistical theory for multipactor

S. Anza,[1] C. Vicente,[1] J. Gil,[1] V. E. Boria,[2] B. Gimeno,[3] and D. Raboso[4]

[1]*Aurora Software and Testing S.L., Edificio de Desarrollo Empresarial 9B, Universidad Politécnica de Valencia, Camino de Vera s/n, 46022 Valencia, Spain*
[2]*Departamento de Comunicaciones-iTEAM, Universidad Politécnica de Valencia, Camino de Vera s/n, 46022 Valencia, Spain*
[3]*Departamento de Física Aplicada y Electromagnetismo-ICMUV, Universitat de València, c/Dr. Moliner, 50, 46100 Valencia, Spain*
[4]*Payloads Systems Division, European Space Agency, 2200-AG Noordwijk, The Netherlands*

This work presents a new and general approach to the real dynamics of the multipactor process: the nonstationary statistical multipactor theory. The nonstationary theory removes the stationarity assumption of the classical theory and, as a consequence, it is able to adequately model electron exponential growth as well as absorption processes, above and below the multipactor breakdown level. In addition, it considers both double-surface and single-surface interactions constituting a full framework for nonresonant polyphase multipactor analysis. This work formulates the new theory and validates it with numerical and experimental results with excellent agreement.

I. INTRODUCTION

Multipactor[1–3] is a resonant nonlinear effect that may occur in high power microwave devices at very low pressures, such as those operating in particle accelerators and satellite subsystems. A multipactor discharge is an electron avalanche in which electrons are accelerated by the electromagnetic fields, successively impacting against the device walls in synchronism with the rf signal frequency. After each impact electrons are released due to secondary emission on the device walls, developing an exponential charge growth and ultimately an electron discharge. Its effects range from signal degradation to the complete destruction of the component. As a consequence, the design of multipactor-free components is a key issue for the space telecommunications industry.

The classical multipactor theory was first developed by Gill and Von Engel in 1948.[2] Since then, the theory has evolved in two main branches. The constant-k theory[2,4,5] and the constant-v theory.[3,6] The former assumes that the emission energy of the secondary electrons is proportional to their impact energy with the proportionality constant k. The latter assumes that the emission energy of the secondary electrons is independent from the impact energy. Both the theories are restricted to single carrier continuous wave operation (the rf signal is composed of only one sinusoid), one-dimensional (1D) electron motion, parallel plates geometry (homogeneous electrostatic field) and a deterministic energy emission of secondary electrons.

It is known that the emission velocity of secondary electrons does not depend on the primary impact energy,[7] which is contrary to the constant-k assumption. However, the secondary emission yield (SEY) parameters and the k constant can be easily tuned to adjust the predicted breakdowns to the experimental results.[8] Therefore, the space industry has adopted this theory for the past years and has applied it to the current multipactor standards.[9]

On the other hand, although the constant-v theory fails to provide reliable breakdown levels,[8] it is aligned with the physics of secondary emission. For this reason, the constant-v theory has prevailed in the scientific community, and more recent works have extended it in order to cover single surface multipactor with magnetic transversal fields[10] and dielectrics,[11] more complicated resonances such as even and hybrid modes[12,13] and more complex geometries, such as irises,[14] rectangular waveguides,[15] and coaxial structures.[16] However, the core of these developments remains that of the classical theory and therefore, they fail to predict experimental multipactor breakdown levels.

Recent studies on statistical multipactor describe a more realistic scenario where the random nature of the electron emission velocity is considered.[17–19] In fact, if the velocity spread becomes large enough, the flight time of electrons can strongly vary from impact to impact, even intercalated with single surface impacts, and still have an overall SEY higher than one. This description of the multipactor phenomenon is known as nonresonant multipactor or polyphase multipactor, giving results which are closer to the experiments.[17,20,21]

This work presents a new nonstationary statistical multipactor theory for single carrier operation, based on the previous work of Vdovicheva *et al.*[17] The nonstationary theory accurately predicts multipactor breakdown levels and models electron multiplication and absorption processes experienced during the multipactor discharge. This theory is valid for both stationary and nonstationary situations, giving a more general and reliable theory to explain the complete multipactor physical process.

First, in order to depict a general view, the status and main limitations of the current multipactor theories are briefly summarized in Sec. II. Then, the new nonstationary theory is presented in Sec. III and finally verified with numerical and experimental results in Secs. IV and V.

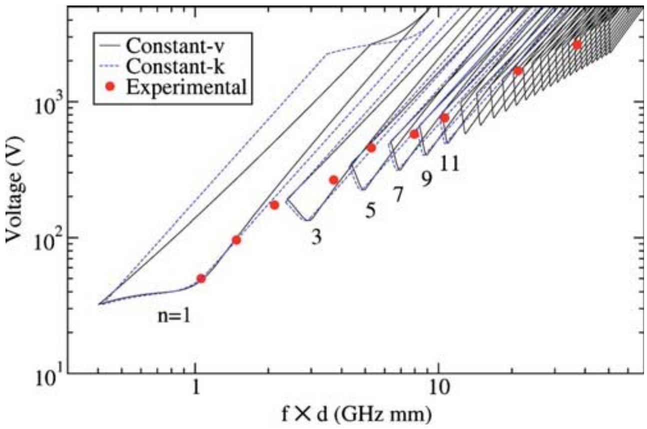

FIG. 1. (Color online) Comparison of constant-k and constant-v plots for $k=5$, electron emission energy $W_0=1.5$ eV, and first and second cross-over energies (energy at which the SEY is equal to 1) $W_1=30$ eV and $W_2=2000$, respectively. Experimental results for silver coating (Ref. 8) are included.

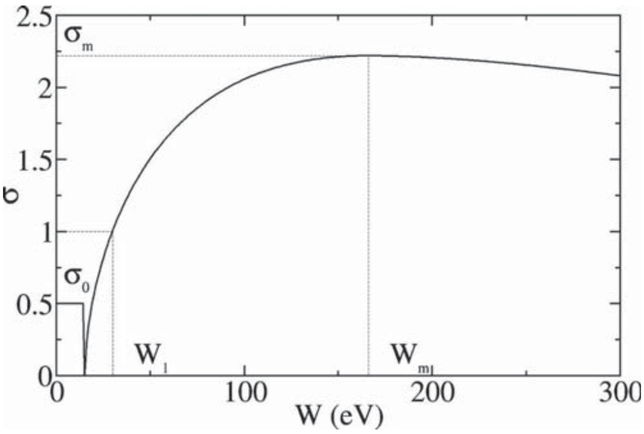

FIG. 2. SEY curve of silver with parameters $W_1=30$ eV, $W_m=165$ eV, $\sigma_m=2.22$, and $\sigma_0=0.5$, where $eW=\frac{1}{2}m_e v^2$ and v is the electron impact velocity. It uses the parametric model of Vaughan (Ref. 22) modified by Vicente (Ref. 23).

II. LIMITATIONS OF THE CURRENT THEORIES

Among the classical theories, the multipactor breakdown levels are typically represented through the multipactor susceptibility curves, firstly introduced by Hatch and Williams.[4] These curves specify the combination of applied voltage, rf frequency (f) and separation between plates or gap (d), needed to start a multipactor discharge. The curves are calculated using the 1D analytical equations of motion of an electron and imposing the conditions of resonance and impact energy, in order to ensure a SEY higher than one (and thus an electron exponential growth). The kind of resonance is set by the multipactor order (or mode), which specifies the number of semiperiods (or cycles) between consecutive electron impacts. The result is a voltage versus $f\times d$ plot, where the regions of multipactor breakdown are delimited for each multipactor order. The susceptibility curves are specific for each material and its respective SEY curve (the SEY depends in turn on the electron impact energy).

Figure 1 shows an example of multipactor susceptibility curves for silver of Ref. 9 whose SEY curve is shown in Fig. 2. The susceptibility curves are similar for the constant-k and constant-v theories, but they considerably differ for the upper voltage limit of the multipactor zones. The experimental breakdown levels of report[8] are superimposed on the susceptibility curves. Whereas breakdown levels are well predicted for multipactor order $n=1$ (first three experimental points), for higher orders, breakdown levels are underestimated. Therefore, although the constant-v theory is widely accepted as the real physical explanation of multipactor phenomenon, it does not provide accurate multipactor susceptibility curves. This is not the case for the constant-k theory, since the aforementioned parameter fitting allows for independently shifting each multipactor order region in order to perfectly match experimental results.[8]

However, even if the constant-k theory is able to match the experimental results through the parameter fitting, it has been severely criticized by some authors,[11] due to its apparently lack of physical basis. Moreover, it seems rather contradictory that a prediction method relies on previous experimental results.

In addition to this, the classical theory models the electron growth for a specific multipactor order as

$$N(t) = N_0\sigma(fd,V_0)^{2ft/n}, \qquad (1)$$

where N_0, $\sigma(fd,V_0)$, and n are the initial number of electrons, the SEY and the multipactor order, respectively, for a specific $f\times d$ product and applied voltage V_0.

In Fig. 3, a band structure of the SEY values can be observed. This implies that there are some regions where the value of the SEY is much higher than one at the breakdown boundary. For instance, for a $f\times d=2$ GHz mm, the SEY value at the breakdown boundary would be close to 2. According to Eq. (1), this leads to a sudden and discontinuous change in the behavior of the electron growth in the neighborhood of the boundary. This seems quite unrealistic since one would expect a SEY equal to one at the boundaries (neither growth nor absorption) and a progressive increment of it as the boundary is exceeded. Furthermore, whilst the experi-

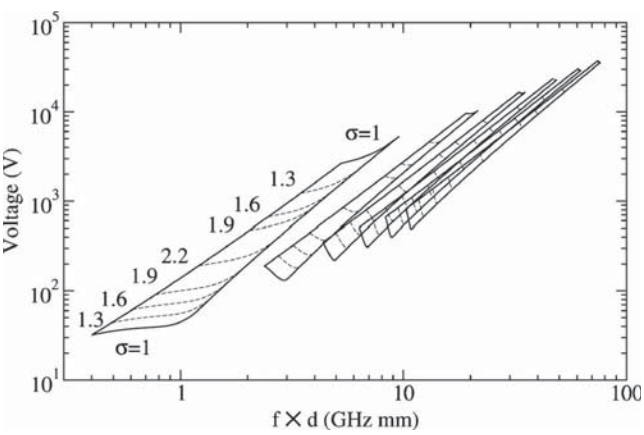

FIG. 3. Constant-v multipactor chart for the first eleven modes and energies $W_0=1.5$ eV, $W_1=30$ eV, and $W_2=2000$ eV. The dotted lines represent the contour plot for the different values of the SEY according to the electron impact energies.

mental measurements show a smooth variation of voltage versus $f \times d$, constant-v curves (also constant-k ones but in a lesser extent) present discontinuities between regions of different multipactor modes. This effect is even higher if the stability condition is also considered, which restricts the multipactor regions to the stable phases where the phase-focusing mechanism is enabled.[3,24] Different explanations have arisen for this mismatching. One of those claims that the presence of hybrid modes "fill" the discontinuities between the main modes.[12,25]

Later, Vdovicheva *et al.*[17] proposed a new statistical theory for multipactor which is also restricted to single carrier and parallel plates. However, for the first time, this theory models the random nature of the emission energy of secondary electrons. Through the statistical theory, the authors justify the broadening, overlapping and suppression of the multipactor regions, and the differences between the classical theory and the experimental results. Subsequently, the statistical theory was extended to study the influence of angular anisotropy electron emission velocity[18] and then particularized for the electromagnetic field distribution of a rectangular waveguide.[19]

However, the main limitation of the statistical theory is the assumption of stationarity.[17] Stationarity implies that only the electrons being emitted with a certain emission phase distribution experience an exponential growth. As a consequence, as time increases, such distribution is favored over the others, the statistics of the multipactor process converging to a stationary solution. Therefore, the statistics of such a situation can be studied within one single period of the rf signal. Unfortunately, the stationarity assumption limits the validity of the results to the regions in which there is electron exponential growth (above the multipactor breakdown level). Hence, the current statistical theory does not model the electron absorption process which occurs below the multipactor breakdown level. This can be of great interest in some applications in which the rf signal presents a nonstationary behavior, such as multicarrier operation,[26] or modulated signal transmission.[27] Moreover, the stationary theory is only able to delimit the multipactor breakdown regions but does not provide information on the rate of electron growth in time.

Finally, the stationary theory only takes into account double surface interaction. It completely neglects single surface impacts, which indeed may represent a high fraction of the total impacts in the multipactor discharge for increasing voltages above the breakdown level. As a consequence, the stationary theory does not provide a full framework for polyphase multipactor.

III. NONSTATIONARY STATISTICAL MULTIPACTOR

The nonstationary statistical theory presented in the following covers the multipactor phenomenon for 1D, parallel plates, electrostatic problems. It is based on the previous and original work on statistical multipactor by Vdovicheva *et al.*[17]

The key point in the statistical theory (stationary and nonstationary) is to assume that the initial velocity of secondary electrons is a random variable, instead of the deterministic value of the classical theory. This simple difference implies a change of paradigm. In the classical theory, an electron in resonance with the electric field would always start with the same phase relative to the field. It would reach the opposite plate in the same transit time, and would be released again with the same starting phase, repeating the trajectory indefinitely in time. On the contrary, if the emission velocity is a random variable, each time an electron is released, its velocity and corresponding transit time will be different, according to its probability density function.

Therefore, within the statistical theory it makes no sense to talk about absolute (and deterministic) resonant phases, multipactor orders, or impact energies, but rather about probabilities: The probability of an electron to be emitted at a certain phase, probability of an electron to reach the opposite plate in a certain transit time or probability to impact with a certain energy.

The main difference between the stationary and this new nonstationary theory is that the latter does not impose stationarity and, therefore, overcomes the current limitations of the former. As a result, the nonstationary theory is valid for all multipactor regions (exponential growth and absorption) and models both double and single-surface impacts.

A. Equations of motion

First, we start from the 1D equations of motion of the classical theory. Let us consider the motion of an electron with charge $-e$ and mass m_e between two infinite parallel plates located at $x=0$ and $x=d$. The sinusoidal electric field of rf frequency f is $E=-E_0 \sin(\omega t)$, where $\omega=2\pi f$. Notice that, for notation purposes, a negative sign has been added to the electric field expression in order to have a positive acceleration. This yields a 1D problem where the electron is accelerated by the Lorentz force, which is equal to $-eE$. The electron maximum speed is considered to be low enough to neglect relativistic effects and, therefore, the acceleration exerted on the electron is given by

$$m_e \ddot{x} = eE_0 \sin(\omega t), \tag{2}$$

where the rf voltage V_0 can be expressed as $V_0=E_0 d$.

The initial conditions at starting time $t=t_s$ are $x|_{t=t_s}=0$ and $\dot{x}|_{t=t_s}=v_0$. From Eq. (2), the rest of the equations of motion can be derived. Concretely, the position of the electron is

$$x = [v_0 + v_\omega \cos(\omega t_s)](t - t_s) + \frac{v_\omega}{\omega}[\sin(\omega t_s) - \sin(\omega t)], \tag{3}$$

where $v_\omega = eV_o/(m_e \omega d)$.

In order to work with dimensionless variables, Eq. (3) is normalized dividing by v_ω/ω. The following notation is used:

$$\begin{aligned} &\xi = \omega x/v_\omega, \quad \varphi = \omega t, \quad \varphi_s = \omega t_s, \\ &\varphi_i = \omega t_i, \quad u = v_0/v_\omega, \quad \lambda = \omega d/v_\omega, \end{aligned} \tag{4}$$

yielding

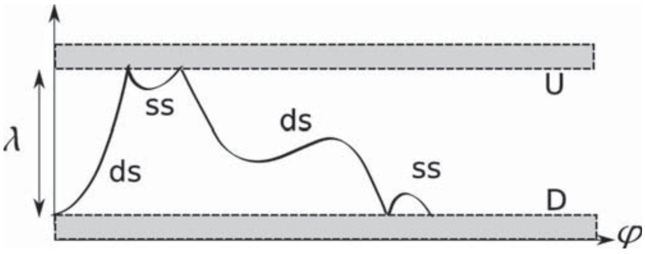

FIG. 4. Nonstationary definitions and conventions. Some possible electron trajectories are depicted and labelled with the corresponding type of interaction, double surface (dd) and single surface (ss).

$$\xi(\varphi, \varphi_s, u) = (u + \cos\varphi_s)(\varphi - \varphi_s) + \sin\varphi_s - \sin\varphi. \tag{5}$$

The phase $\varphi_i = \omega t_i$ at which the electron impacts with the opposite side is the least root of Eq. (5) setting the normalized electron position equal to the normalized gap, i.e., $\xi = \lambda$. This yields

$$\lambda = (u + \cos\varphi_s)(\varphi_i - \varphi_s) + \sin\varphi_s - \sin\varphi_i. \tag{6}$$

Note that Eq. (6) is derived from the classical constant-v theory and establishes the condition for an electron to reach the opposite plate, $\xi = \lambda$ at impacting phase φ_i, with starting phase φ_s, and initial velocity u.

B. Definitions and conventions

Contrarily to the stationary counterpart, the nonstationary theory is not restricted to the study of the probabilities over a period of the rf signal, but rather extends the time window from $t=0$ to infinity. It imposes initial conditions and calculates the time evolution of the different probabilities indefinitely in time. Let as denote each plate as D and U for the boundary conditions $\xi=0$ (down) and $\xi=\lambda$ (up), respectively. Thus two kinds of interactions are considered: double surface (D-U or U-D trajectories) and single surface (D-D and U-U trajectories). All their related parameters are properly labelled as ds and ss, respectively. Figure 4 depicts these concepts.

Table I introduces the most relevant definitions of the nonstationary theory which constitute the basis of its development. In Sec. III C, we will derive the analytical expressions for all of them.

TABLE I. Nonstationary theory definitions.

Impact rate (electrons/radian) in plate U/D at phase φ	$I_{U/D}(\varphi)$
Emission rate (electrons/radian) in plate U/D at phase φ	$C_{U/D}(\varphi)$
Number of electrons at time φ	$N(\varphi)$
Probability density that an electron starting at plate U/D, with starting phase φ, experiences a double/single surface impact in a transit phase τ	$G_{ds/ss,U/D}(\tau\|\varphi)$
SEY of an electron starting at plate U/D, with starting phase φ which experiences a double/single surface impact in a transit phase τ	$\sigma_{ds/ss,U/D}(\tau\|\varphi)$

C. Statistical development

The joint probability density $G(\tau|\varphi_s;\lambda)$ is defined by Vdovicheva *et al.*[17] as the probability that an electron released at phase φ_s impacts with the opposite wall, separated by λ, in a transit phase τ.

In order to construct $G(\tau|\varphi_s;\lambda)$ one departs from the known probability density function of the electron emission velocity u, namely, $f_u(u)$. According to the theorem of transformation of univariate random variables of the statistical theory $G(\tau|\varphi_s;\lambda)$ can be written as

$$G(\tau|\varphi_s;\lambda) = \left|\frac{dg(\tau|\varphi_s;\lambda)}{d\tau}\right| f_u[g(\tau|\varphi_s;\lambda)], \tag{7}$$

where $u = g(\tau|\varphi_s;\lambda)$ must be a monotonic function which expresses u as a function of τ.

From Eq. (6), u can be easily worked out, obtaining a candidate function $g_0(\tau|\varphi_s;\lambda)$

$$u = g_0(\tau|\varphi_s;\lambda) = \frac{\lambda - \sin\varphi_s + \sin(\varphi_s + \tau)}{\tau} - \cos\varphi_s, \tag{8}$$

being $\tau = \varphi_i - \varphi_s$.

By definition, g must be monotonic with τ. However, unfortunately, the candidate g_0 is a nonmonotonic function due to its sinusoidal behavior. The nonmonotonicity of g_0 denotes many solutions of τ for a single release velocity u. This implies that the trajectory of an electron crosses the boundary $\xi=\lambda$ more than once, which is physically impossible (each crossing implies an impact and there cannot be more than one for a trajectory). Therefore, the nonmonotonicity of g_0 can (and must) be removed to obtain g and solve (7). This forces $G(\tau|\varphi_s;\lambda)$ to be 0 in the nonmonotonic intervals of g_0. In addition, g must be greater than a minimum starting velocity (greater than 0) to reach the opposite plate. Vdovicheva *et al.*[17] gives a detailed derivation of $G(\tau|\varphi_s;\lambda)$ and such minimum velocity.

The function $G(\tau|\varphi_s;\lambda)$ is the basis of the statistical theory. From it, Vdovicheva *et al.*[17] formulate the problem by imposing stationarity and find the multipactor breakdown boundaries by solving a homogeneous Fredholm integral equation of the second kind.

The nonstationary theory presented in this work also starts from $G(\tau|\varphi_s;\lambda)$, but follows a different approach, which is detailed next. First, we introduce another definition. $G(\tau|\varphi_s;0)$ is the probability that an electron released at phase φ_s impacts back to the emission surface in a transit time τ (single surface impact). It is constructed in a similar way to Eq. (7)

$$G(\tau|\varphi_s;0) = \left|\frac{dg(\tau|\varphi_s;0)}{d\tau}\right| f_u[g(\tau|\varphi_s;0)], \tag{9}$$

where $u = g(\tau|\varphi_s;0)$ is derived applying $\xi=0$ at impact time $\varphi_i = \omega t_i$ to Eq. (5), and working out the velocity u. This yields the candidate function

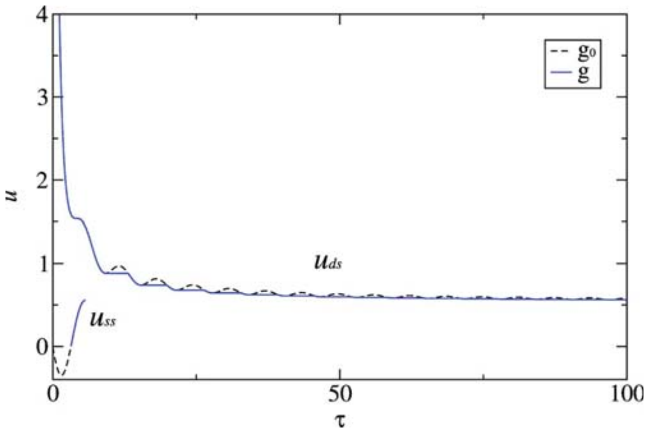

FIG. 5. (Color online) Example of u_{ds} and u_{ss} for $V_0=120$ V, $f=1.64$ GHz, $d=1$ mm, and $\varphi_s=122°$.

$$u = g_0(\tau|\varphi_s;0) = \frac{-\sin\varphi_s + \sin(\varphi_s+\tau)}{\tau} - \cos\varphi_s. \qquad (10)$$

The $g(\tau|\varphi_s;0)$ function can be obtained removing the nonmonotonic intervals of Eq. (10). The minimum ejection velocity for double surface is equal to the maximum ejection velocity for single surface, i.e., $\min(u_{ds})=\max(u_{ss})$, where $u_{ds}\equiv g(\tau|\varphi_s;\lambda)$ and $u_{ss}\equiv g(\tau|\varphi_s;0)$.

Figure 5 shows an example of u_{ds} and u_{ss}. For this specific case, $\min(u_{ds})=\max(u_{ss})=0.55$. Therefore, if the emission velocity u is higher than 0.55 there will be a double surface impact. For lower emission velocities, the electron will suffer a single surface impact.

The $G(\tau|\varphi)$ functions of Table I are defined as

$$\begin{aligned}
G_{ds,D}(\tau|\varphi) &= G(\tau|\varphi_s;\xi)\big|^{\xi=\lambda}_{\varphi_s=\mathrm{mod}(\varphi;2\pi)},\\
G_{ds,U}(\tau|\varphi) &= G(\tau|\varphi_s;\xi)\big|^{\xi=\lambda}_{\varphi_s=\mathrm{mod}(\varphi+\pi;2\pi)},\\
G_{ss,D}(\tau|\varphi) &= G(\tau|\varphi_s;\xi)\big|^{\xi=0}_{\varphi_s=\mathrm{mod}(\varphi;2\pi)},\\
G_{ss,U}(\tau|\varphi) &= G(\tau|\varphi_s;\xi)\big|^{\xi=0}_{\varphi_s=\mathrm{mod}(\varphi+\pi;2\pi)}.
\end{aligned} \qquad (11)$$

The $G(\tau|\varphi)$ functions are periodic with respect to φ with a period of 2π. Note that the direction of the electron normal emission is reversed for opposite plates, and that the rf field changes sign every π radian. Therefore, the G functions for the U and D plates are related by a relative shift of π radians.

The double surface interactions imply that the electron crosses the gap, and therefore $\xi=\lambda$, whereas single surface interactions means that the electron impacts back to the emission surface, $\xi=0$. Therefore the subscripts ds or ss indicate that the solution of $G(\tau|\varphi_s;\xi)$ is particular for $\xi=\lambda$ or $\xi=0$, respectively.

The G_{ds} and G_{ss} functions corresponding to the example of Fig. 5 are presented in Fig. 6. In this case, a Maxwellian distribution for the initial velocity is taken

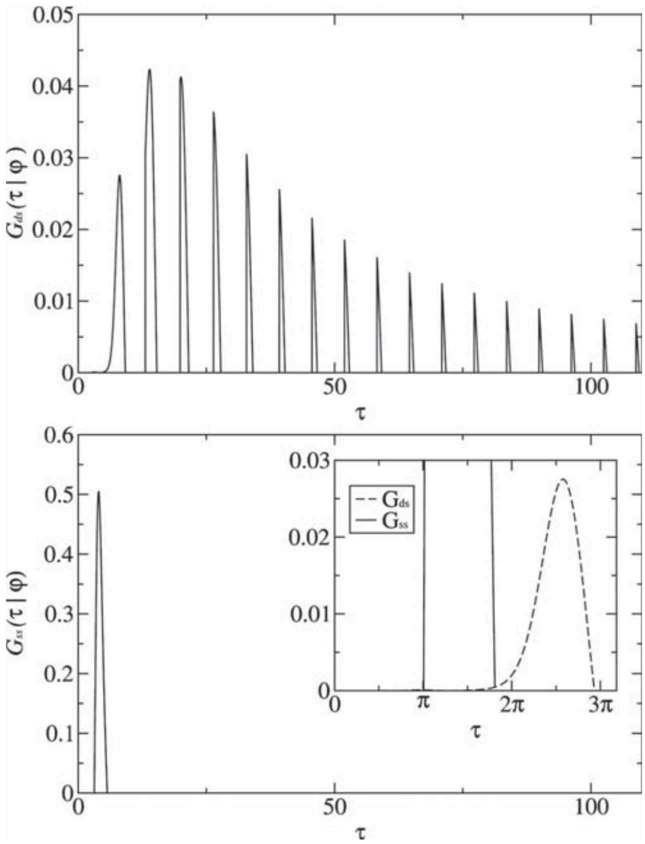

FIG. 6. Example of G_{ds} and G_{ss} probability functions for $V_0=120$ V, $f=1.64$ GHz, $d=1$ mm, $\varphi_s=122°$, and the emission velocity function of Eq. (12). The detailed window of the lower plot shows the superposition of both functions for the first three half-periods of the transit time.

$$f_u = \frac{u v_\omega^2}{v_t^2}\exp\left(-\frac{u^2 v_\omega^2}{2v_t^2}\right), \qquad (12)$$

where v_t is the velocity thermal spread. A value of $W_t=1.5$ eV has been taken for this work, where $W_t=(m_e/2e)v_t^2$ is the thermal emission energy spread. The possible electron transit times are restricted to the regions where the G_{ds} and G_{ss} are not zero. For this specific example, the G_{ss} plot (bottom) shows that the transit time for a single surface impact must lie somewhere in between (approximately) $\tau=\pi$ and $\tau=7\pi/4$. In contrast, all double surface impacts (top) have a transit time higher than $\tau=3\pi/2$. There is a small overlap of both functions in the interval $[3\pi/2-7\pi/4]$, which means that the electrons impacting with such a transit time could have suffered either a double surface interaction or a single surface one, with different probability.

The noticeable difference in amplitude comes from the fact that each function obeys

$$\int_0^\infty G_{ds}(\tau|\varphi)d\tau = P_{ds}(\varphi) \quad\text{and}\quad \int_0^\infty G_{ss}(\tau|\varphi)d\tau = P_{ss}(\varphi),$$

where $P_{ds}(\varphi)$ and $P_{ss}(\varphi)$ are the probability that an electron emitted at φ suffers a double or single surface impact, respectively. Note that $P_{ds}(\varphi)+P_{ss}(\varphi)=1$.

Once the $G(\tau|\varphi)$ functions are obtained, the rest of the definitions given in Table I can be derived in the following

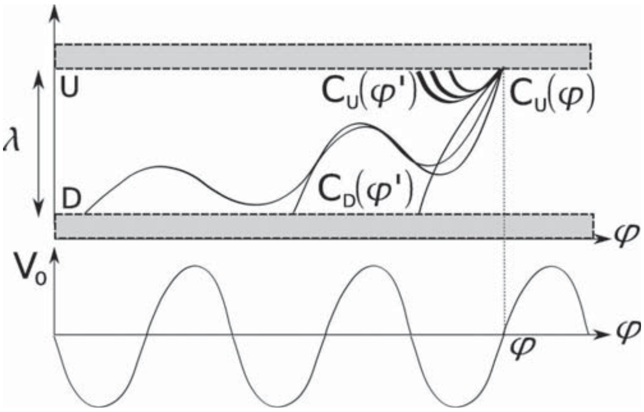

FIG. 7. Dependence of $C_U(\varphi)$ on the previous instants φ'. There are two contributions to $C_U(\varphi)$, electrons emitted from the plate $D[C_D(\varphi')]$, following a double surface interaction, and electrons emitted from plate U $[C_U(\varphi')]$, which experience a single surface interaction.

manner. Let us take the rate of emission at the plate U, $C_U(\varphi)$. At a certain φ, the number of impacting electrons is the result of two contributions: the electrons released from the opposite plate, D, that followed a double surface interaction, and those emitted from the same plate, U, which suffered a single surface interaction (see Fig. 7).

The emission rate at phase φ due to double surface interaction of an electron emitted at phase φ' from the plate D, where $\varphi' < \varphi$ is

$$C_D(\varphi')G_{ds,D}(\varphi-\varphi'|\varphi')\sigma_{ds,D}(\varphi-\varphi'|\varphi'),$$

C_D being the rate of emission at the plate D.

On the other hand, the emission rate at phase φ due to single surface interaction of an electron emitted at phase φ' from the plate U, where $\varphi' < \varphi$ is

$$C_U(\varphi')G_{ss,U}(\varphi-\varphi'|\varphi')\sigma_{ss,U}(\varphi-\varphi'|\varphi').$$

Therefore, the total rate of emission at the top plate and instant φ is the integration of the previous quantities from the initial instant $\varphi'=0$ to the current time $\varphi'=\varphi$, yielding

$$C_U(\varphi) = \int_0^{\varphi} C_D(\varphi')G_{ds,D}(\varphi-\varphi'|\varphi')\sigma_{ds,D} \times(\varphi-\varphi'|\varphi')d\varphi' + \int_0^{\varphi} C_U(\varphi')G_{ss,U} \times(\varphi-\varphi'|\varphi')\sigma_{ss,U}(\varphi-\varphi'|\varphi')d\varphi' + \Psi_U(\varphi), \tag{13}$$

where $\Psi_U(\varphi)$ is the external source of electrons from the plate U.

The rate of emitted electrons at the plate D, $C_D(\varphi)$, can be derived in a similar way yielding

$$C_D(\varphi) = \int_0^{\varphi} C_D(\varphi')G_{ss,D}(\varphi-\varphi'|\varphi')\sigma_{ss,D}(\varphi-\varphi'|\varphi')d\varphi' + \int_0^{\varphi} C_U(\varphi')G_{ds,U}(\varphi-\varphi'|\varphi')\sigma_{ds,U} \times(\varphi-\varphi'|\varphi')d\varphi' + \Psi_D(\varphi). \tag{14}$$

Equations (13) and (14) constitute a system of Volterra integral equations of the second kind with difference kernel. This system has a nontrivial solution only when $\Psi_U(\varphi)+\Psi_D(\varphi)>0$ and $\Psi_U(\varphi)\geq 0$, $\Psi_D(\varphi)\geq 0$ (see chapter 9.3 of Ref. 28). These functions set the initial conditions of the problem. From a physical point of view this implies that electron emission is only possible when there is an external source of electrons, which makes sense, since electrons cannot appear "spontaneously."

Analogously to (13), the remaining definitions of Table I can be expressed as follows:

$$I_U(\varphi) = \int_0^{\varphi} C_D(\varphi')G_{ds,D}(\varphi-\varphi'|\varphi')d\varphi' + \int_0^{\varphi} C_U(\varphi')G_{ss,U}(\varphi-\varphi'|\varphi')d\varphi', \tag{15}$$

and

$$I_D(\varphi) = \int_0^{\varphi} C_D(\varphi')G_{ss,D}(\varphi-\varphi'|\varphi')d\varphi' + \int_0^{\varphi} C_U(\varphi')G_{ds,U}(\varphi-\varphi'|\varphi')d\varphi'. \tag{16}$$

Finally, the number of electrons at time φ is the integration over time of all emitted electrons minus the impacting electrons for both U and D plates, i.e.,

$$N(\varphi) = \int_0^{\varphi} C_U(\varphi') + C_D(\varphi') - I_U(\varphi') - I_D(\varphi')d\varphi'. \tag{17}$$

D. Theoretical analysis

For a given gap, d, signal parameters E and f, SEY function σ (characterizing the material), and seeding function $\Psi(\varphi)$, it is possible to compute all above functions. First, d, E and f are substituted in the equations of motion given in Eqs. (4) and (5). The $G_{ds}(\tau|\varphi)$ and $G_{ss}(\tau|\varphi)$ functions are computed using Eqs. (8), (7), (10), and (9). Later, the system of Volterra integral equations constituted by Eqs. (13) and (14) is solved (in most cases with standard numerical techniques[29]) finding the electron emission functions C_U and C_D. Then, I_U and I_D are obtained by simple integration of Eqs. (15) and (16) and finally, N is given by Eq. (17).

Figure 8 shows an example for the Maxwellian emission velocity distribution given in Eq. (12). The SEY model is taken from paper,[26] with the SEY parameters of silver given in Ref. 9: $\sigma_0=0.5$, $\sigma_m=2.22$, $W_1=30$ eV, and $W_m=165$ eV (see Fig. 2). The external seeding has been set to

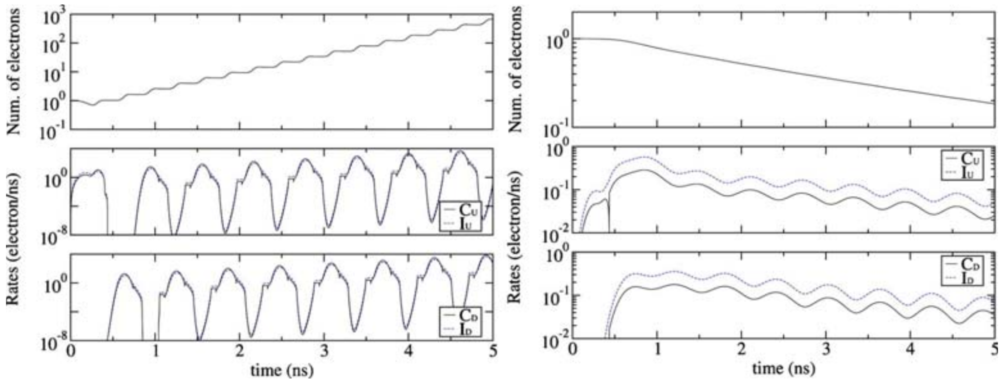

FIG. 8. (Color online) Time evolution of the electron population and emission and impact rates for both plates for $V_0=120$ V (left) and $V_0=10$ V (right), with $f=1.64$ GHz and $d=1$ mm.

$$\Psi_U(\varphi)=\Psi_D(\varphi)=\tfrac{1}{2}\delta(\varphi),$$

where $\delta(\varphi)$ is the Dirac delta function. This means that seeding electrons are only injected at $\varphi=0$.

In both cases, a repetitive pattern can be appreciated. Notice how, after a transitory interval at the beginning, the curves associated to the U and D plates evolve to adopt a similar shape but shifted in time (exactly π radians). The electron population, $N(t)$, is altered whenever there is an impact in any of the plates. Therefore, the variation of the electron population curve perfectly agrees with the peaks of the emission and impact curves (C_U and C_D for the former and I_U and I_D for the latter).

This can be better appreciated in the $V_0=120$ V case [Fig. 8 (left)] where the rf voltage is above the breakdown level. In general, the rate of electron emission is higher than the electron impact (or absorption), and therefore there is an overall increase of charge with time, following an exponential trend.

The $V_0=10$ V case [Fig. 8 (right)] shows a situation where the rf voltage is below the breakdown level. In this case the impact curves are always higher than the emission ones and therefore there is an overall destruction of charges. Hence, the electron population decreases in time.

It may be also useful to define SEY and multipactor order parameters equivalently to the classical Theory. The instantaneous SEY is the ratio between the total emission rate divided by the total impact rate, thus

$$\sigma_i(\varphi)=\frac{C_{(\varphi)}}{I(\varphi)}, \tag{18}$$

where $C(\varphi)=C_U(\varphi)+C_D(\varphi)$ and $I(\varphi)=I_U(\varphi)+I_D(\varphi)$. On the other hand, the instantaneous order is computed as the statistical expectation of the flight time for all kind of interactions divided by the total impact rate

$$\begin{aligned}n_i(\varphi)=\frac{1}{\pi I(\varphi)}\Bigg[&\int_0^{\varphi}(\varphi-\varphi')C_D(\varphi')G_{ds,D}(\varphi-\varphi'|\varphi')d\varphi'\\&+\int_0^{\varphi}(\varphi-\varphi')C_U(\varphi')G_{ds,U}(\varphi-\varphi'|\varphi')d\varphi'\\&+\int_0^{\varphi}(\varphi-\varphi')C_D(\varphi')G_{ss,D}(\varphi-\varphi'|\varphi')d\varphi'\\&+\int_0^{\varphi}(\varphi-\varphi')C_U(\varphi')G_{ss,U}(\varphi-\varphi'|\varphi')d\varphi'\Bigg].\end{aligned} \tag{19}$$

Finally, in an interval $\Delta\varphi$, average quantities are defined as

$$\sigma_{\text{av}}(\varphi)=\frac{\int_{\varphi}^{\varphi+\Delta\varphi}\sigma_i(\varphi')I(\varphi')d\varphi'}{\int_{\varphi}^{\varphi+\Delta\varphi}I(\varphi')d\varphi'}, \tag{20}$$

and

$$n_{\text{av}}(\varphi)=\frac{\int_{\varphi}^{\varphi+\Delta\varphi}n_i(\varphi')I(\varphi')d\varphi'}{\int_{\varphi}^{\varphi+\Delta\varphi}I(\varphi')d\varphi'}, \tag{21}$$

for the SEY and multipactor order, respectively. These two parameters characterize the electron growth, since, although the exact solution can be found integrating Eq. (17), an easier and faster approximation for an interval $\Delta t=\Delta\varphi/\omega$ is given by

$$N(t+\Delta t)\approx N(t)\sigma_{\text{av}}^{2f\Delta t/n_{\text{av}}}. \tag{22}$$

IV. NUMERICAL SIMULATIONS

The numerical results have been obtained with the full-wave electromagnetic solver tool FEST3D,[23,30] which also incorporates a three-dimensional (3D) particle-in-cell (PIC) multipactor module. FEST3D is able to simulate arbitrary 3D structures with inhomogeneous electromagnetic field distributions. However, in order to compare the results with the present theory, the simulations have been restricted to 1D electron motion and homogeneous electric field. The FEST3D multipactor module computes the electron trajectories, deter-

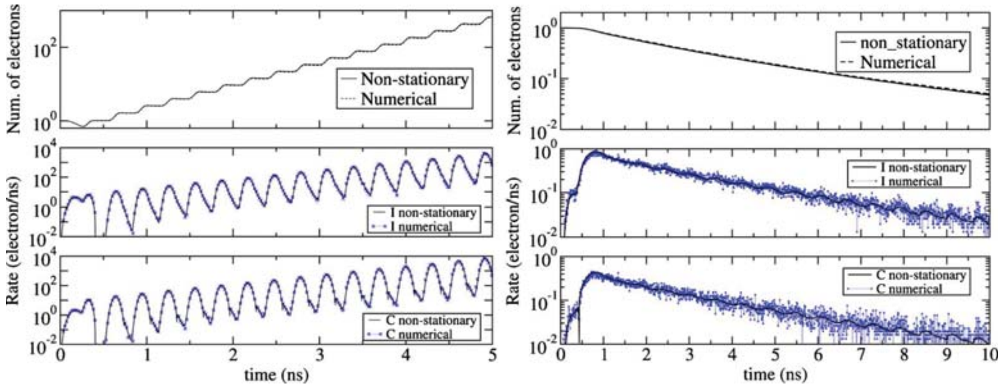

FIG. 9. (Color online) Time evolution of electron population and emission and absorption rates for $V_0=120$ V (left) and $V_0=10$ V (right), with $f=1.64$ GHz and $d=1$ mm.

mines all electron impacts (both single and double surface) and records the associated flight time and SEY for each one. The simulations have been done for a number of 50 000 initial particles, to have enough samples for a good statistical analysis. During the simulation, the particles can be created or destroyed depending on the impact energy. The results have been normalized to have one initial electron, in order to compare with the analytical results.

The numerical equivalent SEY is the average SEY for all impacts

$$\sigma_{eq} = \frac{\sum_{i=1}^{i=N_t} \sigma_i}{N_t}, \tag{23}$$

where N_t is the total number of impacts, and σ_i is the SEY at impact i, respectively. The numerical equivalent multipactor order is defined as the average travel time, divided by half period of the rf signal

$$n_{eq} = 2f \frac{\sum_{i=1}^{i=N_t} t_i}{N_t}, \tag{24}$$

where t_i is the flight time for impact i.

V. RESULTS

All the simulations and analytical results have been carried out assuming the Maxwellian distribution of Eq. (12) for the electron initial velocity and $W_t=1.5$ eV. The SEY model is that of Ref. 31. The SEY parameters are for the silver given in paper,[9] i.e., $\sigma_m=2.22$, $W_1=30$ eV, and $W_m=165$ eV with $\sigma_0=0.5$ (see Fig. 2).

Figure 9 shows the time evolution of a multipactor discharge. Two different scenarios are considered. First, a case with a voltage above the breakdown level in which there is an electron exponential growth (left); and a nonresonant, nonstationary situation below breakdown, in which there is an overall electron absorption (right). The analytical evolution in time of the electron population N, total rate of impact I and total rate of electron emission C, given by Eq. (17) and Eqs. (13)–(16), respectively, are plotted and compared with numerical simulations, with identical initial conditions. Besides the inherent numerical noise of the simulator due to the limited number of samples (electrons), it can be observed an excellent agreement between numerical simulations and the nonstationary theory.

The instantaneous SEY and order defined by Eqs. (18) and (19) have been also compared with numerical simulations in Fig. 10. Again, a very good agreement between

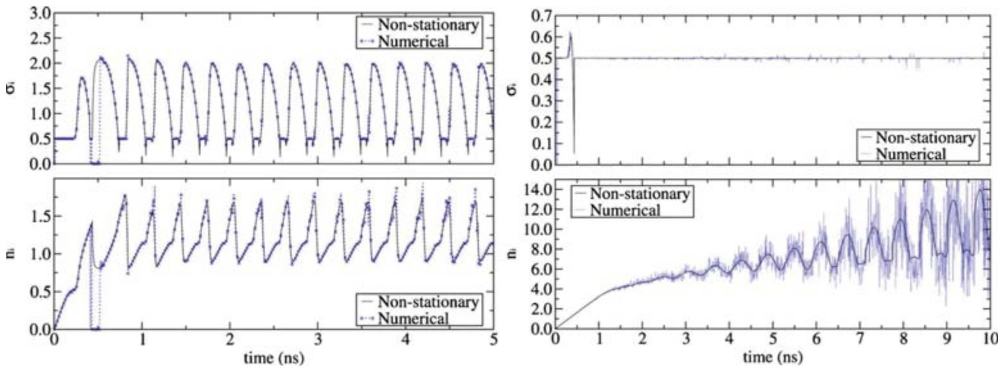

FIG. 10. (Color online) Electron population and instantaneous SEY and order or $V_0=120$ V (left) and $V_0=10$ V (right), with $f=1.64$ GHz, $d=1$ mm, and $\varphi_s=122°$.

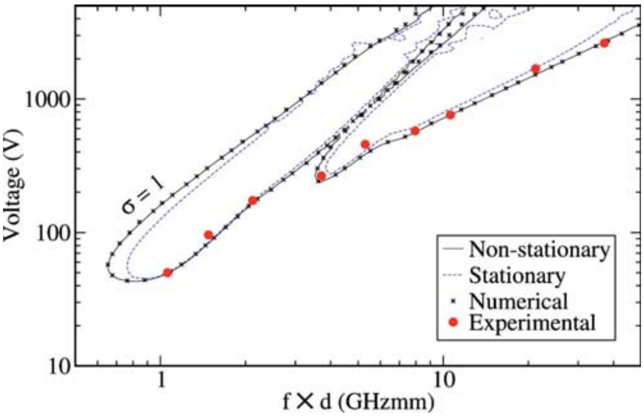

FIG. 11. (Color online) Analytical and numerical Multipactor breakdown boundaries for silver. Experimental results are included.

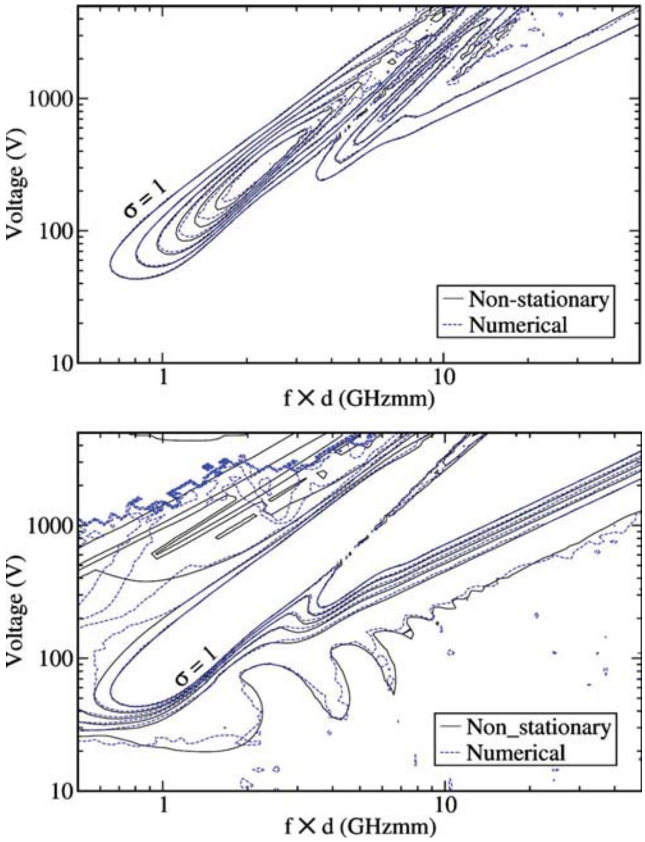

FIG. 12. (Color online) Analytical equivalent SEY calculated with Eq. (21) for silver and numerical simulations with FEST3D for $\sigma > 1$ (top) and $\sigma < 1$ (bottom).

theory and numerical results is observed. Here, the stationarity of the above-breakdown case is evidenced (left). After an initial transitory, both the SEY and order evolve towards a periodic structure. Nevertheless, in the below-breakdown situation (right), although the SEY keeps constant (due to the low impact energy of the electrons), the multipactor order diverges and indefinitely increases in time, which implies a clear nonstationary condition. This occurs because electrons with higher emission energy impact earlier and get quickly absorbed. Therefore, as time increases, the surviving electrons are those with lower emission energies and higher transit times, which implies an increasing multipactor order with time. The current stationary theory cannot model this situation, whereas the new nonstationary one matches the numerical simulations with extremely good agreement. Notice that the random dispersion on the numerical simulations for increasing time is due to the fact that a large amount of electrons have been already absorbed and therefore there are less samples available to produce smooth averages.

The multipactor boundaries calculated with stationary (reproducing the formulation of Ref. 17) and nonstationary theories together with numerical simulations are plotted in Fig. 11. The analytical boundaries are delimited by $\sigma_{\mathrm{av}}=1$, given by Eq. (21). The numerical ones are set by $\sigma_{eq}=1$ [Eq. (23)].

The nonstationary theory curve shows a better agreement with numerical simulations than the stationary one, concretely for the upper boundary regions and high $f \times d$ product, where the influence of single surface impacts is higher. The three curves are coincident for the regions close to the breakdown level. The experimental breakdown levels from report[8] are also plotted, showing an excellent agreement with the theory. This evidences the capability of the statistical theories to predict the multipactor breakdown level in the whole $f \times d$ range, in contrast with the classical theories which are restricted to the first multipactor order.

SEY contour plots can be represented in Voltage versus $f \times d$ maps using Eq. (20). The isoline of $\sigma=1$ represent the multipactor breakdown boundary. Figure 12 shows such representation for a $\sigma > 1$ (top) and $\sigma < 1$ (bottom). The isolines are plotted with a 0.2 and 0.1 step, respectively, starting from 1.

In Fig. 12 (bottom), while the results for the region below the breakdown boundary perfectly agrees with numerical results, the regions above show a dissimilar trend. This is due probably to the numerical noise of the simulations for very high fields, and the limited number of time samples in the electron trajectory computation.

These multipactor maps, coming from the nonstationary statistical theory, show a different structure of the SEY compared with the classical theory (see Fig. 3). In contrast to the discontinuous band structure of the classical theory, the nonstationary theory shows a constant SEY value of 1 at the breakdown boundary which varies smoothly with the rf voltage. This is successfully contrasted with numerical simulations.

Finally, the contour plot for the equivalent order of the nonstationary theory (21) is shown in Fig. 13. The nonstationary theory is valid for any kind of material, provided that its SEY parameters are available. In this case, a custom material with SEY parameters $\sigma_0=0.5$, $\sigma_m=2.12$, $W_1=25$ eV, and $W_m=364$ eV is used. The contour lines are plotted for odd integer values starting from 1. In the multiplication region, the traditional band structure is observed, whereas for the region below breakdown the lines deflect to almost get vertically aligned with the plot. This is because for decreas-

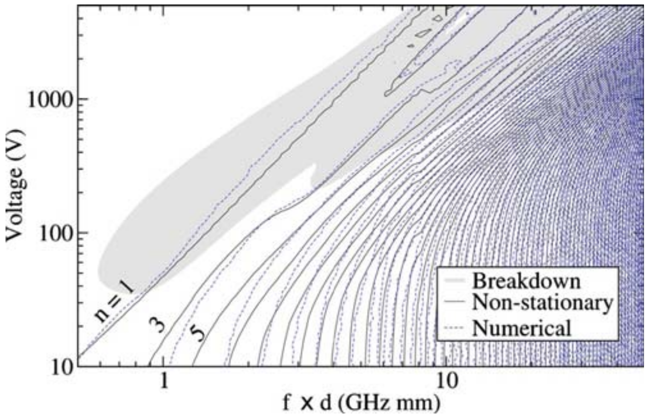

FIG. 13. (Color online) Analytical equivalent order calculated with Eq. (21) for custom material and numerical simulations with FEST3D.

ing voltages, the transition time depends almost exclusively on the gap d and the thermal spread v_t, and thus, the dependence on $f \times d$ is broken. The theory and numerical results match quite well in the multiplication region. Below that, the definition of a multipactor order is not valid anymore, because the process is then not stationary and the instantaneous multipactor order indefinitely increases in time.

VI. CONCLUSIONS

A new nonstationary statistical multipactor theory has been presented. It is based on previous works on statistical multipactor but overcoming some of its limitations. Specifically, the stationarity assumption has been removed and single surface interactions have been incorporated to the model. In consequence, this new theory is able to accurately predict the time evolution of the most relevant parameters characterizing the multipactor process.

This theory provides realistic multipactor susceptibility charts including SEY and order contour plots for the whole V versus $f \times d$ region, characterizing the dynamics of the discharge. These plots reveal a different SEY structure than the one predicted by the classical theory. Instead of a discontinuous sharp band structure, the SEY shows a smooth transition at the breakdown boundaries, where it has a value of 1. This result is radically different from the one given by the classical theory and depicts a progressive and continuous change in the electron growth as the boundary is exceeded. This constitutes a much more realistic scenario of the electron dynamics.

The theory has been verified with numerical results coming from a PIC multipactor simulator and experimental results available in literature. The agreement between the theory, the numerical and the experimental results is excellent.

To the knowledge of the authors, this is the first theory which provides a framework for the study of a full polyphase electron interaction for both an exponential electron growth and a nonstationary electron absorption (when multipactor conditions are not met). This is of particular importance in nonstationary multipactor processes such as multicarrier operation and signal modulation. Therefore, this theory may constitute the basis for further study of multipactor in more complicated geometries and signals.

ACKNOWLEDGMENTS

The authors would like to thank ESA/ESTEC for having funded this research activity through the Contract "Study of High Order Modes and Fringing Fields in Multipactor Effect" (Contract No. 1-5918/08/NL/GLC) and to the Ministerio de Ciencia e Innovacion (Spain) for the support through the "Programa Torres Quevedo" Contract No. PTQ05-02-02759.

[1] P. Farnsworth, J. Franklin Inst. **218**, 411 (1934).
[2] E. W. B. Gill and A. von Engel, Proc. R. Soc. London, Ser. A **192**, 446 (1948).
[3] J. Vaughan, IEEE Trans. Electron Devices **35**, 1172 (1988).
[4] A. Hatch and H. Williams, J. Appl. Phys. **25**, 417 (1954).
[5] A. Hatch and H. Williams, Phys. Rev. **112**, 681 (1958).
[6] H. M. Wachowski, El Segundo Technical Operations Aerospace Corporation, Technical Report No. TDR-269(9990)-5, El Segundo, California, 1964.
[7] M. Furman and M. Pivi, Phys. Rev. ST Accel. Beams **5**, 124404 (2002).
[8] A. Woode and J. Petit, ESTEC Technical Report No. 1556, Noordwijk, 1989.
[9] *Space Engineering: Multipacting Design and Test*, edited by ESA-ESTEC (ESA Publication Division, The Netherlands, 2003), Vol. ECSS-20-01A.
[10] S. Riyopoulos, D. Chernin, and D. Dialetis, Phys. Plasmas **2**, 3194 (1995).
[11] R. Kishek, Y. Lau, L. Ang, A. Valfells, and R. Gilgenbach, Phys. Plasmas **5**, 2120 (1998).
[12] A. Gilardini, J. Appl. Phys. **71**, 4629 (1992).
[13] A. Kryazhev, M. Buyanova, V. Semenov, D. Anderson, M. Lisak, J. Puech, L. Lapierre, and J. Sombrin, Phys. Plasmas **9**, 4736 (2002).
[14] V. E. Semenov, E. Rakova, R. Udiljak, D. Anderson, M. Lisak, and J. Puech, Phys. Plasmas **15**, 033501 (2008).
[15] V. E. Semenov, E. I. Rakova, D. Anderson, M. Lisak, and J. Puech, Phys. Plasmas **14**, 033501 (2007).
[16] R. Woo, J. Appl. Phys. **39**, 1528 (1968).
[17] N. K. Vdovicheva, A. G. Sazontov, and V. E. Semenov, Radiophys. Quantum Electron. **47**, 580 (2004).
[18] N. K. Vdovicheva, A. G. Sazontov, V. A. Sazontov, and V. E. Semenov, Radiophys. Quantum Electron. **49**, 368 (2006).
[19] A. G. Sazontov, V. A. Sazontov, and N. K. Vdovicheva, Contrib. Plasma Phys. **48**, 331 (2008).
[20] A. Sazontov, M. Buyanova, V. Semenov, E. Rakova, N. Vdovicheva, D. Anderson, M. Lisak, J. Puech, and L. Lapierre, Phys. Plasmas **12**, 053102 (2005).
[21] I. A. Kossyi, G. S. Lukyanchikov, V. E. Semenov, E. I. Rakova, D. Anderson, M. Lisak, and J. Puech, J. Phys. D **41**, 065203 (2008).
[22] J. Vaughan, IEEE Trans. Electron Devices **36**, 1963 (1989).
[23] C. Vicente, M. Mattes, D. Wolk, H. L. Hartnagel, J. R. Mosig, and D. Raboso, *Proceedings of the 5th International Workshop on Multipactor, RF and DC Corona and Passive Intermodulation in Space RF Hardware* (ESTEC, Noordwijk, The Netherlands, 2005), pp. 11–17.
[24] A. Gilardini, J. Appl. Phys. **78**, 783 (1995).
[25] A. Kryazhev, M.S. thesis, Chalmers University of Technology, Göteborg, Sweden, 2002.
[26] S. Anza, C. Vicente, B. Gimeno, V. E. Boria, and J. Armendariz, Phys. Plasmas **14**, 082112 (2007).
[27] P. Zuccarello, A. González, G. Piñero, and M. de Diego, *Proceedings of*

the 4th International Workshop on Multipactor, RF and DC Corona and Passive Intermodulation in Space RF Hardware (ESTEC, Noordwijk, The Netherlands, 2003), pp. 469–473.
[28] A. D. Polyanin and A. V. Manzhirov, *Handbook of Integral Equations* (CRC, Cleveland, 1998).
[29] W. H. Press, S. A. Teukolsky, W. T. Vetterling, and B. P. Flannery, *Numerical Recipes, The Art of Scientific Computing* (Cambridge University Press, New York, 2007).
[30] S. Anza, C. Vicente, D. Raboso, J. Gil, B. Gimeno, and V. E. Boria, *IEEE International Microwave Symposium* (IEEE, Atlanta, 2008), pp. 1095–1098.
[31] C. Vicente, M. Mattes, D. Wolk, H. L. Hartnagel, J. R. Mosig, and D. Raboso, *Microwave Symposium Digest, IEEE MTT-S International* (IEEE, Long Beach, California, 2005), Vol. 2, pp. 1055–1058.